Title
Alumina-coated Ag nanocrystal monolayers as surfaceenhanced Raman spectroscopy platforms for the direct spectroscopic detection of water splitting reaction intermediates

Authors
Ling, Xing Yi
Yan, Ruoxue
Lo, Sylvia
et al.

Peer reviewed

TABLE OF CONTENTS (TOC)

Authors are required to submit a graphic entry for the Table of Contents (TOC) in conjunction with the manuscript title. This graphic should capture the readers' attention and give readers a visual impression of the essence of the paper. Labels, formulae, or numbers within the graphic must be legible at publication size. Tables or spectra are not acceptable. Color graphics are highly encouraged. The resolution of the figure should be at least 600 dpi. The size should be at least $50 \text{ mm} \times 80 \text{ mm}$ with a rectangular shape (ideally, the ratio of height to width should be less than 1 and larger than 5/8). One to two sentences should be written below the figure to summarize the paper. To create the TOC, please insert your image in the template box below. Fonts, size, and spaces should not be changed.

Alumina Coated Ag Nanocrystal Monolayer as Surface-Enhanced Raman Spectroscopy Platforms for Direct Spectroscopic Detection of Water Splitting

Reaction Intermediates

Xing Yi Ling[1,#, †], Ruoxue Yan[1,#, ††],

Sylvia Lo[1], Dat Tien Hoang[1], Chong Liu[1], Melissa A. Fardy[1], Sher Bahadar Khan[2], Abdullah M. Asiri[2], Salem M. Bawaked[2],

Peidong Yang[1,2]

1. University of California Berkeley, United States

2. King Abdulaziz University, Saudi Arabia

umbers. The

Page N

A novel Ag-alumina hybrid SERS platform has been designed for the spectroscopic detection of surface reactions in steady state.

font is ArialMT 16 (automatically inserted by the publisher)

Provide the authors' website if possible.

1

Alumina Coated Ag Nanocrystal Monolayer as Surface-Enhanced Raman Spectroscopy Platforms for Direct Spectroscopic Detection of Water Splitting Reaction Intermediates

Xing Yi Ling[1,#,†⎕], Ruoxue Yan[1,#,††], Sylvia Lo[1], Dat Tien Hoang[1], Chong Liu[1], Melissa A. Fardy[1], Sher Bahadar

Khan[2], Abdullah M. Asiri[2], Salem M. Bawaked[2], Peidong Yang[1,2] (⎕)

[1] Department of Chemistry, University of California, Berkeley, CA, United States
[2] Center of Excellence for Advanced Materials Research (CEAMR), King Abdulaziz University, Jeddah 21589, P.O. Box 80203, Saudi Arabia

† Present address: Division of Chemistry and Biological Chemistry, School of Physical and Mathematical Sciences, Nanyang

Technological University, Singapore

†† Present address: Department of Chemical and Environmental Engineering. University of California, Riverside, CA, United States # These authors contributed equally to this work

ABSTRACT

A novel Ag-alumina hybrid SERS platform has been designed for the spectroscopic detection of surface reactions in steady state. Single crystalline and faceted silver (Ag) nanoparticles with strong light scattering were prepared in large quantity, which enables their reproducible self-assembly into large scale monolayers of Raman sensor arrays by

Langmuir-Blodgett technique. The close packed sensor film contains high density of sub-nm gaps between sharp edges of Ag nanoparticles, which created large local electromagnetic field that serve as "hot spots" for SERS enhancement. The SERS substrate was then coated with a thin layer of alumina by atomic layer deposition to prevent charge transfer between Ag and the reaction system. Photocatalytic water-splitting reaction on a monolayer of anatase TiO_2 nanoplates decorated with Pt co-catalyst nanoparticles were employed as a model reaction system. Reaction intermediates of water photo-oxidation were observed at the TiO_2/solution interface under UV irradiation. The surface-enhanced Raman vibrations corresponding to peroxo, hydroperoxo and hydroxo surface intermediate species were observed on TiO_2 surface, suggesting the photooxidation of water on these anatase TiO_2 nanosheets may be initiated by a nucleophilic attack mechanism.

KEYWORDS

Surface-Enhanced Raman Spectroscopy, Water Splitting Reaction, Reaction Intermediates, Ag nanocrystals.

———————————————

Address correspondence to p_yang@berkeley.edu

2

1. Introduction

Photocatalysis of overall water splitting, which converts cheap and abundant resources such as solar energy and water to hydrogen and oxygen [1], is considered one of the most important chemical reactions for clean and sustainable energy generation [2]. If solar energy can be captured and converted efficiently, it would be one of the best candidates to replace non-renewable fuel reserves and to provide 15TW energy required annually to sustain human civilization [3]. Significant efforts have been focused on developing better photocatalysts to increase the solar absorption efficiency and broaden the range of solar spectrum captured [1, 2]. Nanostructured semiconductors[4] (e.g. GaP, InGaN and GaN:ZnO) and metal oxides (e.g. TiO_2, $NaTaO_3$, WO_3, $SrTiO_3$), which offers large surface area for both co-catalyst loading and chemical reactions and tunability in their electronic structures [5], are being extensively studied for improved photocatalytic performance [2]. In addition to the band gap engineering in these semiconductors, it is equally important to understand the kinetics of the water splitting reaction. In particular, characterization of reaction pathways and mechanisms, and the verification of surface intermediate species are of utmost importance to provide valuable insights to the nature of photocatalytic reaction at the molecular level, and to enable rational design of photocatalytic systems towards improved activity, selectivity and efficiency [6-9].

Many techniques, such as surface-enhanced Raman spectroscopy (SERS) [10-13], X-ray photoelectron spectroscopy (XPS) [14], infrared (IR) spectroscopy [15-18], sum frequency generation (SFG) [19] have been used to identify active sites and surface reaction intermediates in catalytic reactions [20-25]. Among them, SERS, which utilizes optically excited coherent oscillations of conduction electrons on a rough metal surface to create drastic enhancement in the Raman signals of absorbed molecules, is a unique spectroscopic detection technique that offers both surface-sensitive and chemical-bond specific information, ideal for the direct sensing of surface intermediates of chemical reactions. In addition, the ability of SERS to access low frequency vibration modes from 1100 cm^{-1} down to ~100 cm^{-1} allows direct detection of surface intermediate formation on metal and metal oxide catalysts, such as M=O, M-O-H and M-O-M, making it highly promising for in-situ spectroscopic study of heterogeneous catalysis reactions.

The SERS sensitivity has been reported to reach a signal enhancement factor of 10^{14}, with a potential for single-molecule detection [26-28]. Such high sensitivity is enabled by the recent advances in both the shape and size control in plasmonic nanocrystal synthesis for improved crystallinity, tunable scattering performance and sharp edges/corners that offer local "hot spots" for SERS enhancement [29-31], as well as the assembly techniques for patterning these SERS active nanocrystals into coupled aggregates for further enhancement of electromagnetic field from the nanometer sized inter-particle gaps [29, 32-37]. For the purpose of the direct detection of surface reaction intermediates during photocatalysis, large area nanocrystal SERS substrates with homogeneous and strong electromagnetic field enhancement are required. Previously, we have demonstrated that using the Langmuir Blodgett (LB) technique, it is possible to assemble of faceted Ag nanocrystals with sharp corners into close-packed large area SERS substrate with sub-nm inter-particle gaps that have enhancement factor (EF) of up to 10^8 and are optically homogeneous to perform quantitative ultra-sensitive SERS arsenic sensing with a detection limit

3

of ~1ppb [38]. These substrates should also offer an ideal platform for the SERS detection of reaction intermediates in solution.

Here, we designed large area alumina coated Ag nanocrystal monolayer as novel SERS platforms for real time spectroscopic monitoring of surface intermediates during heterogeneous catalytic reactions to advance the fundamental understanding of reaction mechanisms. Our strategy is to integrate the 2D close-packed assembly of Ag nanocrystals, which serves as the ultra-sensitive SERS platform, with an ultra-thin atomic layer deposited alumina layer, working as the protective coating to prevent Ag nanocrystals from directly taking part in the reaction (Fig. 1(a)). Such platform would offer direct access to the vibrational fingerprints of surface intermediate species of nanocrystalline catalysts deposited on the film during photocatalytic reactions.

As a model reaction system to demonstrate the feasibility of our design, a photocatalyst monolayer of TiO_2 nanoplates decorated with co-catalyst Pt nanoclusters was overlaid onto the Ag hybrid SERS platform (Fig. 1). Water oxidation reaction was performed under UV irradiation and surface intermediates on TiO_2 surface, including surface peroxo, hydroperoxo and hydroxo, were successfully
identified on these SERS platforms.

2. Results and discussion

Ag nanocube-alumina hybrid SERS platforms have been developed for probing of surface intermediate species of the overall photocatalytic water-splitting reaction on TiO_2 nanocrystal surface. The fabrication of the SERS platform starts with the large scale synthesis of single crystalline Ag nanoparticles with well-defined {001} faceted cubic structure. These cubic Ag nanoparticles of ~ 100 nm displayed strong scattering properties, with distinctive localized surface plasmon resonance (LSPR) of dipole and quadrupole (Fig S-1 in the Electronic Supplementary

edges and corners that serve as "hotspot" to enhance the sensitivity of SERS detection, has a reported enhancement factor of up to 10^5 [37-39].

The Ag nanocubes were then assembled into close-packed monolayer SERS substrate by Langmuir-Blodget method. Figure 1(c) shows SEM micrograph of monolayer of Ag nanocubes, with sub-nanometer inter-particle gaps. The small gaps between the neighboring nanocubes could concentrate the electromagnetic field through inter-particle coupling. In our previous studies, a 10^3-10^4 times higher enhancement in SERS sensitivity than that of a single Ag nanoparticle has been observed on LB assembled monolayers [38, 40] with consistent spectral responses throughout the sample. It should be noted that the assembled Ag nanoparticles were coated with a surfactant, poly(vinyl)pyrrolidone (PVP), evidenced from the strong PVP signals of the Raman spectrum from as-prepared Ag nanocubes (Fig. S-2(a) in the ESM).
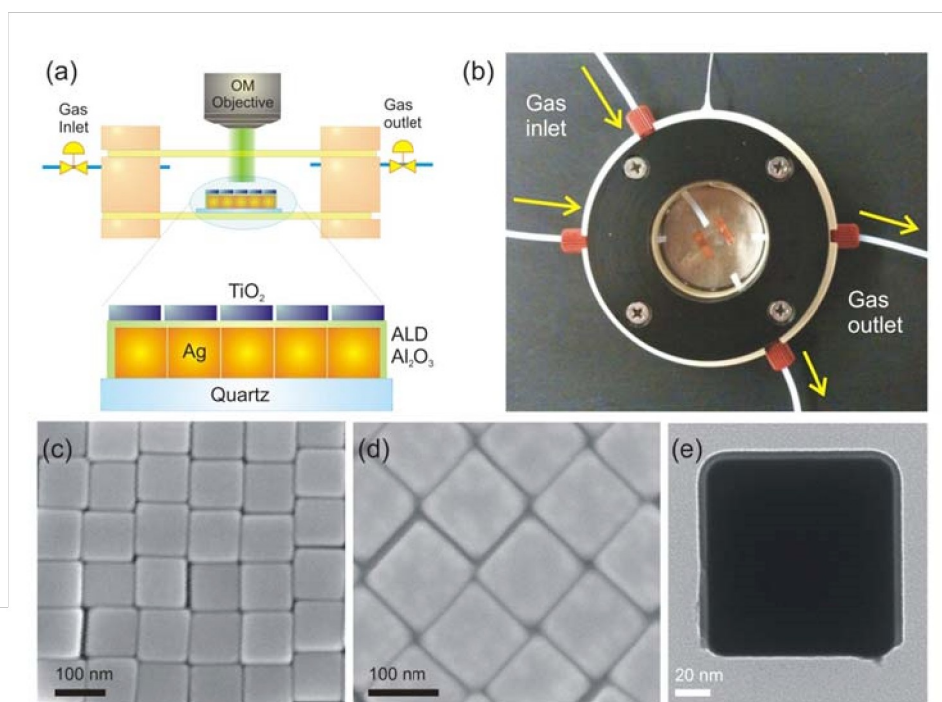

Figure 1. (a) Scheme and (b) photograph of the experimental cell, where Ag nanocube Langmuir-Blodgett film was first coated with a ~ 3 nm of Al_2O_3 by ALD deposition, follow by Langmuir-Blodgett assembly of square TiO_2 nanocrystals. The sample was placed on the bottom quartz slide, and deoxygenated solution was added. The chamber was closed and blown with Ar gas for at least 15 min prior to UV irradiation. SEM images of (c) Ag nanocube film made by Langmuir-Blodgett technique and (d) Ag nanocube film after Al_2O_3 coating. (e) TEM image of an Al_2O_3-coated Ag nanocube peeled off from quartz slide.

Material (ESM)). The nanocubes, which have sharp

The presence of PVP is vital for the dispersion and stabilization of nanocrystals during the LB assembly process. For SERS measurement, however, a clean chemical background was essential, thus additional cleaning steps were carried out to remove PVP from the nanocube monolayer. The Ag LB layer was first cleaned in O_2 plasma for a few seconds, upon which, the PVP fingerprint in Raman spectrum was significantly reduced (Fig. S-2(a) in the ESM). In principle, the reduction of PVP signal can be attributed to the removal of PVP from the Ag surface, and/or by reduction of SERS enhancement as a result of Ag oxidation. To distinguish the two effects, the Ag substrate was rinsed in an ethanol solution of aminothiophenol, which is known to form a self-assembled monolayer on Ag surface. The absorbed aminothiophenol exhibited very strong Raman signals on the O_2 plasma cleaned SERS substrate. A comparison of the Raman signals on aminothiophenol-coated substrates with and without O_2 plasma treatment (Fig. S-2(b) in the ESM) showed comparable Raman signals, indicating that mild O_2 cleaning procedure did not significantly deteriorate the SERS substrate, which is consistent with the report by Xia et al [41].

To prevent Ag nanocubes from directly taking part in the photocatalysis reaction and to inhibit Ag oxidation, atomic layer deposition (ALD), which allows the high quality conformal coating of metal oxide, was performed immediately upon the cleaning process to render an ultra-thin layer of Al_2O_3 on the surface of Ag nanocubes (Fig. 1(d)). To protect the sharp edges and corners of the nanocubes from rounding and welding with their neighbors, low temperature Al_2O_3 deposition (80 °C) was performed. The TEM image in Figure 1(e) was collected by peeling off an Al_2O_3-coated Ag cube from quartz surface. 10 cycles of alumina ALD yielded an Al_2O_3 coating of about 3 nm, which is sufficient to act as a physical barrier to prevent direct contact between the electrolyte and metallic Ag, while preserving SERS activity of the sensors.

The thermodynamic potential for overall water-splitting is 1.23 eV. Hence, a semiconductor capable of overall photocatalytic water-splitting must have a band-gap greater than 1.23 eV with conduction/valence band positions straddle the water-splitting redox potentials. Few semiconductors meet such requirements, among which anatase TiO_2, with a band-gap of 3.2 eV, has been a popular material for this purpose. In addition, high surface area TiO_2 nanoparticles can be produced in large quantities with high crystallinity or low defect density [42, 43]. With state-of-the-art particle morphology engineering, it is now possible to selectively expose the high surface energy facets of TiO_2 nanoparticles to further boost their catalytic activity.
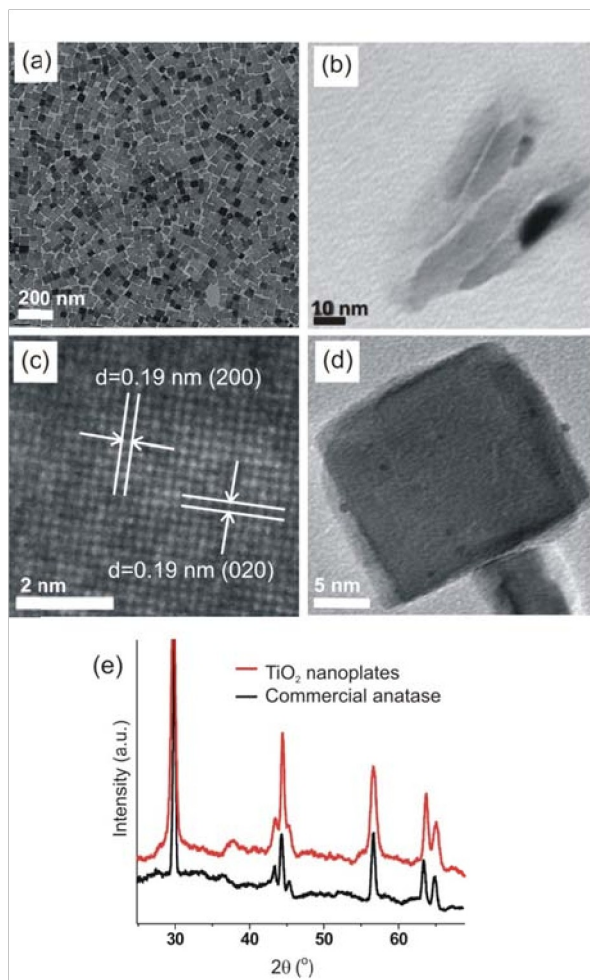

Figure 2. TEM images of (a) a Langmuir-Blodgett film of TiO_2 nanocrystals, (b) cross-sectional view of TiO_2 nanoplates, (c) high resolution TEM image of TiO_2 nanoplate, indicating the presence of two sets of lattice fringes (1.9 Å) that corresponds to the {200} and {020} facets, (d) TiO_2 nanocrystal deposited with Pt nanoparticles. (e) XRD of TiO_2 nanoplates as compared to commercially available anatase powder.

Here, phase pure anatase TiO_2 nanoplates that are 30-50 nm in width (Fig. 2(a)) were synthesized using a solvothermal method. Cross-sectional TEM image of these TiO_2 nanoplates showed that the nanoplates were 5-10 nm in height (Fig. 2(b)). Two sets of lattice fringes (1.9 Å) that corresponds to the {200} and {020} planes were measured from the high-resolution TEM image (Fig. 2(c)), clearly indicating the exposed square surfaces of the nanoplates in the LB film were the {001} facets. X-ray diffraction (XRD) measurement further confirmed the anatase structure of the as-synthesized TiO_2 nanoplates, showing characteristic anatase TiO_2 diffraction peaks of

2θ of 29.5°, 44.1° and 56.3°, originated from (101), (004) and (200) reflections, respectively (Fig. 2(e)). The {001} facets are predicted to have higher surface energy (0.90 J/m^2) as compare to {100} (0.53 J/m^2) and {101} (0.44 J/m^2), and are believed to be better for certain catalytic application [44-46]. The as-synthesized TiO_2 nanoparticles often form aggregates in aqueous solution. To ensure homogeneous close-packed assembly of these TiO_2 nanoplates on the SERS platform, ligand exchange was necessary. Both carboxylic acids and phosphonic acids are known to be organic anchors for tailoring surface properties of TiO_2. However, carboxylic acids may be gradually oxidized on photocatalytic TiO_2 in the presence of water and UV radiation; which may in turn lower the stability of TiO_2 [47]. Thus tetradecylphosphonic acid (TDPA), which is more stable under our reaction condition, was chosen as the exchange ligand in this study. After the ligand exchange, TiO_2 nanoplates form a stable suspension in water. To facilitate H_2 production from TiO_2 nanoplates, they were decorated with Pt nanoclusters by photodeposition (Fig. 2(d)).

For direct SERS monitoring of the photocatalytic water-splitting reaction, a monolayer of TiO_2 nanoplates was assembled onto the Ag-Al_2O_3 platforms via LB technique. As shown in the TEM image (Fig. 2(a)), the LB assembly of TiO_2 nanoplates formed a close-packed 2D monolayer with good dispersity. The LB technique also enabled the large area (>cm^2) assembly of closed-packed 2D TiO_2 nanoplates film, making it an ideal platform for photocatalytic reaction.

To elucidate the SERS effects of our hybrid Ag-Al_2O_3 platform on the overlaying TiO_2 nanoplate monolayer, Raman spectra were compared between LB assembled close-packed TiO_2 films overlaid on the SERS platform and on plain silicon. As shown in Figure 3(a), when using Ag SERS platform, three distinguish peaks at 400, 519, and 643 cm^{-1} which represents anatase fingerprint of O-Ti-O bending and Ti-O stretching modes were clearly observed [42, 48].
Raman measurements performed on random positions on the TiO_2/Ag platforms have all exhibited the characteristic anatase TiO_2 features reproducibly. On silicon substrate, however, the Raman signals of the 5-nm thick TiO_2 nanoplate monolayer assembled under identical conditions were too weak to show resolvable peaks under the same Raman measurement condition. The results highlight the sensitivity of Ag nanocubes and the spatial consistency of our Ag-alumina SERS platforms. It is also noted that Raman fingerprints of remnant organic molecules on the TiO_2 nanoplates were

observed in the spectrum window of 1200 – 1800 cm^{-1} using our Ag SERS platform (Fig. S-2(c) in the ESM).

To ensure an inert atmosphere for the overall photocatalytic water-splitting reaction, an airtight homemade reactor was used that allows a closed reaction system and Ar purging before the reaction starts (Fig. 1(b)). The reactor has upper and lower quartz windows to allow Raman laser and UV illumination to access the sample, so that steady-state SERS signals of the TiO_2 film can be monitored at different stages of the reaction (Figure 1). Figure 3(b) shows the SERS spectra of the TiO_2 nanoplates film in contact with deoxygenated alkaline solution of pH 10 after UV irradiation as a function of the illumination time (t=40, 60 and 90 mins), with the TiO_2 film prior to UV irradiation taken as a spectral reference, which shows typical TiO_2 anatase fingerprints, with a clean spectrum window between 650 -1100 cm^{-1}. During the course of the reaction, no Ag-O vibrations was observed in the region between 217 – 487 cm^{-1} [49], indicating the Al_2O_3 coating has effectively shielded the metallic Ag from taking part in photocatalysis reaction.

Prominent spectral changes started after 60 mins of UV irradiation, when the surface coverage of the intermediate species of photo water-splitting accumulated to over the SERS detection limit and several new bands emerged in the spectrum window of 650-1100 cm^{-1}. With increasing irradiation time, the intensity of these new bands increased, indicating a further increase in surface coverage of corresponding surface species and after 90 mins of illumination, the spectrum has become quite stable, indicating a steady-state has been reached (Fig. S-3 in the ESM). At t = 90 mins, a few distinguished bands around 680 cm^{-1}, 830 cm^{-1}, 980 cm^{-1}, and 1050 cm^{-1} were clearly observed. The peaks at 830 cm^{-1}, 980 cm^{-1}, and 1050 cm^{-1} were asymmetric, indicating the existence of multiple peaks within each of these envelops, and they were deconvoluted for further peak analysis. The peak at ~ 830 cm^{-1} (Fig. 4(a)) was associated with the O–O stretching modes from the reaction intermediates on the TiO$_2$ surface. It was dominated by a strong peak centered at 835 cm^{-1}, which can be assigned to the O-O stretching of the
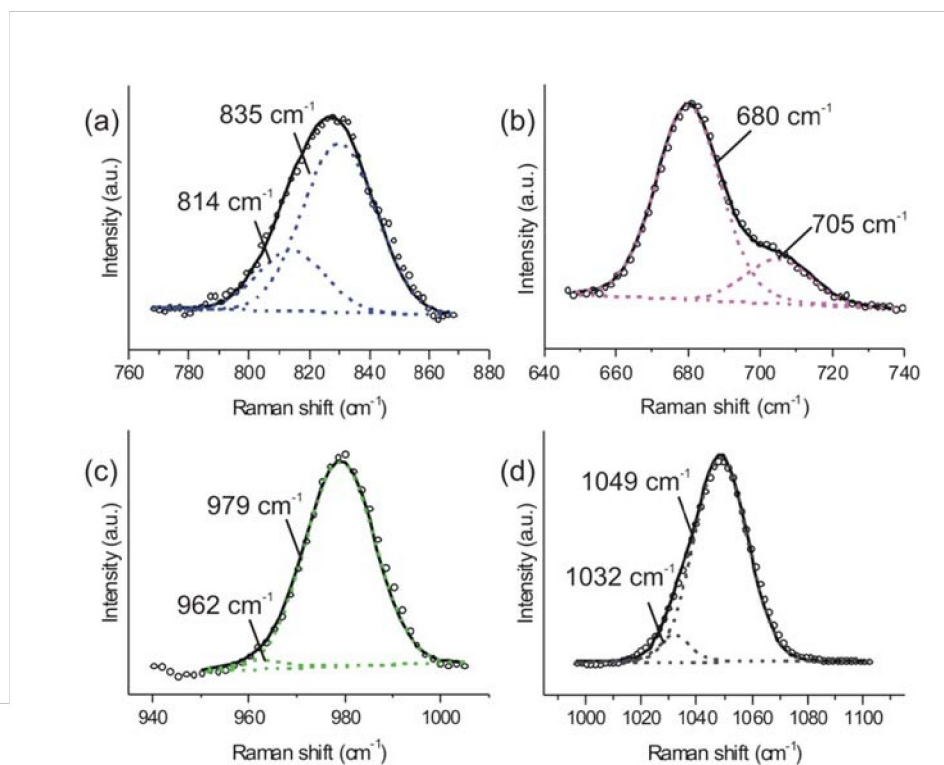

Figure 4. (a - d) Deconvoluted SERS spectra of surface species on TiO$_2$ nanoplates after 90 min irradiation at pH 10 condition.

bridge type surface peroxo species Ti-O-O-H [9]. A strong support to this assignment is an IR study of the exposure of Ti-silicalite molecular sieves (TS-1) to 30% H_2O_2, which gave two IR bands at 837 and 877 cm^{-1} [50]. The former 837 cm^{-1} band was assigned to the O-O stretching mode of a surface hydroperoxo species (TiOOH) and the latter to free H_2O_2 molecules. There also existed a weaker shoulder peak at 814 cm^{-1}, which can be attributed to the O-O stretching of another surface peroxo species: Ti-O-O-Ti [9]. The replacement of H with Ti in the surface peroxide moved this shoulder peak ~20 cm^{-1} higher up in vibrational frequency. Similar observation was reported by Nakato et al [9], who observed the O-O stretchings of Ti-O-O-Ti and Ti-O-O-H at 812 cm^{-1} and 838 cm^{-1} in their in-situ FTIR measurements of Pt-loaded rutile TiO_2 during photo water reduction. These peroxide species were believed to be the primary intermediates of water oxidation from photo-generated holes.

The sensitivity of our Ag nanocube SERS platform has enabled the detection of additional reaction intermediate bands at 680 cm^{-1}, 980 cm^{-1} and 1050 cm^{-1}, which were not previously observed spectroscopically. The 680 cm^{-1} band, emerging at 60 mins as a shoulder on the high frequency side of the 643 cm^{-1} anatase phonon peak and growing rapidly from 60 to 90 mins, consists of a major band at 680 cm^{-1} and a shoulder band at 705 cm^{-1} (Fig. 4(b)). These two bands are not associated with the Raman fingerprint of TiO_2, anatase or rutile [48, 51]. This is the first time these peaks were observed experimentally and the origins are not yet clear. These two peaks are not likely due to either the -OH bending vibrations from surface –OH groups or –OOH groups, which existed in the spectrum range of 750 -1450 cm^{-1}, or the O-O stretching in surface -O-O-H groups, which is also higher in frequency (860-900cm^{-1}) [7]. They are closer in frequency to the collective Ti-O stretching vibrations of the TiO_6 octahedron in anatase TiO_2, in the spectral range of 510-640 cm^{-1} [48], and is possibly due to the Ti-O stretching on the TiO_2 surface as a result of photo-induced surface structure distortion during the reaction [46, 47, 54, 55]. Although the origin of the 680cm^{-1} peak are not clear at the moment, the fact that it only existed under UV-radiation and their intensity overwhelms the original anatase peaks suggested that they were closely associated with photo-activated surface species which has high surface coverage.

The broader 980 cm^{-1} band (Fig. 4(c)) can be resolved into a small peak at 962 cm^{-1} and a prominent peak at 979 cm^{-1}. The small peak at 962 cm^{-1} can be attributed to the production of a surface peroxo species, $Ti(O_2^{2-})$ during water splitting reaction [7, 52]. The presence of O_2^{2-} can be attributed to the reduction of adsorbed O_2 on TiO_2 surface. Prior to UV irradiation (t = 0 min), no O_2^{2-} species

was observed, indicating that the reaction solution was well deoxygenated. During the water-splitting reaction, free oxygen was produced. These free O_2 molecules can bind to the under-coordinated Ti atoms at the TiO_2 surface, which carry a partial positive charge due to the missing O, and behave like a strong electron acceptor by inducing an unoccupied state near the valence band maximum of anatase TiO_2. They were subsequently reduced to negatively charged peroxo species, as predicted by Bonapasta et.al. with ab-initio calculation of O_2 interaction with TiO_2 {100} anatase surface. The double negative charge on $Ti(O_2^{2-})$ will strongly attract H$^+$ and favor the formation of hydroperoxo groups. Indeed, the peak at 979 cm^{-1} indicated the presence of a surface hydroperoxo group stabilized by water, or [Ti-OOH$^-$ + nH$_2$O] [7]. The OOH group is tightly bounded to the Ti surface with a short Ti-O distance of 1.83Å and a desorption enthalpy of -2.09 eV [7]. In the proposed mechanism for O_2 oxidation in acidic solution [7], the negative charge of the surface OOH$^-$ groups would favor further protonation and the formation of surface bound H_2O_2. However, Ti-OOH$^-$ is expected to be more stable under higher pH against further protonation, which would contribute to the absence of O-O stretching peak of surface absorbed H_2O_2, which would appear at 877 cm^{-1}. This is consistent with an in-situ FTIR study of surface intermediates of photocatalytic O_2 reduction on TiO_2 thin film, where no surface absorbed H_2O_2 were observed in basic condition [52].

The peak(s) in the region between 1010 – 1080 cm^{-1} is not symmetrical, indicating the presence of more than one vibration frequencies, i.e. 1032 cm^{-1} and 1049 cm^{-1} (Fig. 4(d)). These bands suggested that two types of OH terminal groups are present, i.e., bridged OH group (OH-b) and surface terminal (OH-t) groups. The former is a two-fold coordinated OH group involving an oxygen atom bridging between two Ti atoms. The bridged oxygen atom forms hydrogen bond with an H atom from water, giving rise to an O-H bending mode at 1032cm^{-1}. The vibration frequency at 1049 cm^{-1} can be assigned to the surface OH terminal groups on the TiO_2 surfaces [7]. Unlike bridged OH-b that connects two adjacent Ti atoms, the terminal OH group of surface OH-b group is bonded to only one Ti surface atom. It should be noted that these peaks are not present in dark, possibly because that at pH 10, which is well above the point of zero charge of anatase TiO_2 (~5.9-6.0), the surface Ti-O-Ti and under-coordinated Ti exist in their deprotonated form. This argument is supported by detailed studies on surface oxygen species on TiO_2 in a pH range of 2.3-11.7 by internal reflection FTIR spectroscopy [53], which reports that protonated bridging oxygen Ti-OH$^+$-Ti exists below pH 4.3, and Ti-OH from dissociative

absorption of H_2O on an oxygen vacancy only present at pH 4.3 to 10.7. At pH 10, the population of all protonated surface oxygen species would be low. The high intensity of these OH peaks under UV radiation suggests high surface population of these species on TiO_2 surface and their importance in photo-oxidation
of water.

The observation of these reaction intermediates, including Ti-OH (terminal OH-t and bridged OH-b groups), Ti-O-O-Ti, Ti-O-OH clearly indicated the oxygen oxidation half reaction can be resolved spectroscopically by using our hybrid Ag SERS platforms. This observation supported nucleophilic attack mechanism for photo-oxidation of water [8]. The water oxidation is initiated by the nucleophilic attack of water on a surface Ti-O-Ti site, accompanied by the absorption of a photo-generated hole to form [Ti-O• HO-Ti], which were then coupled upon oxidation to form Ti-O-O-Ti (as observed in 814 cm^{-1}). Resultant Ti-O-O-Ti binds with an additional water molecule to form Ti-O-OH (835 cm^{-1}) and Ti-OH (1032 cm^{-1} and 1049 cm^{-1}),
which then release free O_2 through further oxidation.

3. Conclusion

We have demonstrated a novel Ag/Al_2O_3 hybrid SERS platform for the detection of surface reaction intermediate species in heterocatalysis and photocatalysis reactions. Shape controlled Ag nanocrystals were assembled into a close-packed monolayer with high density of small inter-particle gaps as "hotspots" for SERS detection, onto which a thin layer of alumina was coated using ALD to serve as a physical and chemical barrier to prevent Ag from participate in the catalytic reaction. The eligibility of such ultrasensitive SERS platforms for steady-state spectroscopic detection of surface intermediates on heterogeneous catalysts were demonstrated with an overall water splitting reaction system, featuring anatase TiO_2 nanoplates with predominant high surface energy {001} facets as photocatalysts for water oxidation and Pt nanoparticles decorated on them as catalysts for water reduction. Surface intermediates, including surface hydroperoxo (Ti-O-OH), terminal and bridged hydroxo (Ti-OH) and peroxo (Ti-O-O-Ti), were experimentally identified under UV radiation using the SERS platform. Many of these species were not previously observed spectroscopically. Our observations are in good agreement with the nucleophilic attack mechanism of water photo-oxidation on TiO_2 surface. Direct detection of reaction intermediates is essential in advancing our fundamental understanding of the reaction mechanism of heterogeneous catalysis and the molecular interactions at

the catalyst's surface. Such efforts will also provide valuable insights to the
improvement of catalytic efficiency and selectivity.

4. Materials and Methods

4.1 Generals.

1,5-pentanediol (98%), silver nitrate (97%), polyvinylpyrrolidone (Mw 55,000), copper chloride, dioctylamine, potassium tetrachloroplatinate(II) (98%) and benzyl alcohol (>99%) were purchased from Sigma Aldrich. Titanium (IV) isopropoxide (99.9%) was obtained from Alfa Aesar. Scanning electron micrographs were obtained using a field emission scanning electron microscope (FESEM, JEOL 6340F). Images were obtained with an
operating voltage of 5 kV.

4.2 Ag nanoparticle synthesis.

Ag cubes (100 nm) were synthesized according to our previously reported procedure [54]. In brief, silver nitrate (0.20 g) and copper(II) chloride (0.86 mg) were dissolved in 1,5-pentanediol (10 mL) in a glass vial. In a separate vial, PVP (MW 55 000 amu, 0.10 g) was dissolved in 1,5-pentanediol (10 mL). All solutions were dissolved in ultrasonic baths. The resulting silver nitrate solution is a slightly opaque yellow-orange solution. Using a temperature-controlled silicone oil bath,
1,5-pentanediol (20 mL) was heated in a flask for 10 min at 190 °C. The precursor solutions were then injected into the hot reaction flask at the following rates: 500 μL of the silver nitrate solution every minute and 250 μL of the PVP solution every 30 s. For nanocubes, this addition was stopped once the solution turned opaque (~ 14 min).

4.3 TiO2 nanoplate synthesis and Pt nanocluster impregnation.

A solution of 0.17 M titanium (IV) isopropoxide, 1.2 M dioctylamine and 0.2 M deionized water in benzyl alcohol was prepared. The as-made solution was placed in a Teflon liner which was then sealed into a solvothermal autoclave (Parr Instruments). The autoclave was heated at 185 °C for 24 h. The reaction was then cooled down and the white precipitates were obtained. The ligand exchange was carried out by vigorously stirring TiO_2 nanoplates in a chloroform solution of n-tetradecylphosphonic acid (TDPA) for 2 hrs. Excess TDPA was removed from TiO_2 suspension solution via a series of centrifugation and re-dispersion cycles. The particles were then exposed to UV

lamp to remove bounded surfactant from the nanoparticle surface. The resulting pellet was dried in a gentle argon-flow overnight. The TiO_2 nanoparticles were impregnated with Pt-nanoclusters by a photodeposition process: the dried particles were redispersed in deionized water, to which Potassium tetrachloroplatinate(II) ($M_{Pt}:M_{TiO2}$=3:100) was added. The solution was exposed to a UV-lamp for 6 hours under stirring, after which the nanoparticles were collected by centrifugation, and dried overnight in a gentle argon-flow.

4.4 Self-assembly of nanoparticles and alumina deposition.

Nanoparticle assembly was carried out with a Nima Technology Langmuir-Blodgett (LB) trough [55-57]. The Ag nanocrystals were first suspended in ethanol and chloroform (volume ratio 2: 3) was added dropwise to a volume of approximately 1 – 2 ml. The suspension of particles in mixture of chloroform and ethanol was added to the surface of the water in the LB trough dropwise, and the chloroform was allowed to evaporate for a minimum of 30 mins. The film was then compressed at 10 cm^2min^{-1} until the surface pressure reached 14 $mNcm^{-2}$. During the compression, the reflection of nanoparticle suspension changed from green to metallic color, indicating a densely packed layer of nanocubes has been formed. This close-packed film was transferred to quartz and/or silicon substrates by a mechanical dipper moving at 2 $mm.min^{-1}$. The Ag substrates were treated with O_2 plasma momentarily for surfactant removal. Immediately after the O_2 plasma treatment, a ~ 3 nm film of Al_2O_3 was grown over the array by 10 cycles of atomic layer deposition with trimethylalumina and water as precursors (home built system). Finally, the Pt-photodeposited TiO_2 nanoparticles were assembled onto the Ag-alumina hybrid array using the same LB procedure. Similar to Ag nanocubes, TiO_2 nanoplates were first dispersed on the water surface of the LB trough, and then slowly compressed into close-packed monolayer film. The 2D ordered TiO_2 nanocrystals were transferred onto the Ag SERS platform for overall water splitting reaction.

4.5 SERS Measurement.

For the water splitting reaction, a home-made flow cell was fabricated. The flow cell is consistent of a top and a bottom quartz window, a Teflon spacer that separate the windows and gas/solution inlets and outlets. The Pt/TiO_2 deposited Ag hybrid SERS platform was placed on the bottom quartz window, onto which deoxygenated water at pH 10 (unless otherwise stated) was added. The cell was then topped with the top quartz window and sealed with O-rings. Two inlets and two outlets are imbedded in the spacer for the purpose of purging and/or chemical injection. They were plugged to ensure a close reaction system during reaction. The flow cell was purged with argon prior to experiment for at least 15 mins. A UV LED lamp (M365L2, Thorlab,Inc, P = 360 mW, □ = 365 nm) was employed as the light source for the photocatalysis reaction. The incident power density on the sample was approximately 20 mW/cm^2. Raman spectra were obtained with a laser confocal Raman system (Horiba JY LabRAM HR; diode pumped-Nd:YAG laser, 532 nm, 0.2W), with an Olympus SLMPLN 50□ long distance objective. The typical acquisition time is 30s.

Acknowledgements

Electronic Supplementary Material: Supplementary material (further details of the dark field and Raman spectroscopy measurements) is available in the online version of this article at
http://dx.doi.org/10.1007/s12274-***-****-*
(automatically inserted by the publisher).

References

[1] Maeda, K.; Domen, K., Photocatalytic Water Splitting: Recent Progress and Future Challenges. J. *Phys. Chem. Lett.* **2010**, *1*, 2655-2661.

[2] Kudo, A.; Miseki, Y., Heterogeneous photocatalyst materials for water splitting. *Chem. Soc. Rev.* **2009**, *38*, 253-278.

[3] Lewis, N. S.; Nocera, D. G., Powering the planet: Chemical challenges in solar energy utilization. *Proc. Natl. Acad. Sci. U. S. A.* **2006**, *103*, 15729-15735.

[4] Maeda, K.; Xiong, A.; Yoshinaga, T.; Ikeda, T.; Sakamoto, N.; Hisatomi, T.; Takashima, M.; Lu, D.; Kanehara, M.; Setoyama, T.; Teranishi, T.; Domen, K., Photocatalytic Overall Water Splitting Promoted by Two Different
Cocatalysts for Hydrogen and Oxygen Evolution under Visible Light. *Angew. Chem. Int. Ed.* **2010**, *49*, 4096-4099.

[5] Kuykendall, T.; Ulrich, P.; Aloni, S.; Yang, P., Complete composition tunability of InGaN nanowires using a combinatorial approach. *Nature Mater.* **2007**, *6*, 951-956.

[6] Sivasankar, N.; Weare, W. W.; Frei, H., Direct Observation of a Hydroperoxide Surface Intermediate upon Visible Light-Driven Water Oxidation at an Ir Oxide Nanocluster Catalyst by Rapid-Scan FT-IR Spectroscopy. *J. Am. Chem. Soc.* **2011**, *133*, 12976-12979.

[7] Mattioli, G.; Filippone, F.; Amore Bonapasta, A., Reaction Intermediates in the Photoreduction of Oxygen Molecules at the (101) TiO2 (Anatase) Surface. *J. Am. Chem. Soc.* **2006**, *128*, 13772-13780.

[8] Imanishi, A.; Okamura, T.; Ohashi, N.; Nakamura, R.; Nakato, Y., Mechanism of Water Photooxidation Reaction at Atomically Flat TiO2 (Rutile) (110) and (100) Surfaces: Dependence on Solution pH. *J. Am. Chem. Soc.* **2007**, *129*, 11569-11578.

[9] Nakamura, R.; Nakato, Y., Primary Intermediates of Oxygen Photoevolution Reaction on TiO2 (Rutile) Particles, Revealed by in Situ FTIR Absorption and Photoluminescence Measurements. *J. Am. Chem. Soc.* **2004**, *126*, 1290-1298.

[10] Tian, Z.-Q.; Ren, B.; Chen, Y.-X.; Zou, S.-Z.; Mao, B.-W., Probing electrode/electrolyte interfacial structure in the potential region of hydrogen evolution by Raman spectroscopy. *J. Chem. Soc., Faraday Trans.* **1996**, *92*, 3829-3838.

[11] Niaura, G., Surface-enhanced Raman spectroscopic observation of two kinds of adsorbed OH− ions at copper electrode. *Electrochim. Acta* **2000**, *45*, 3507-3519.

[12] Heck, K. N.; Janesko, B. G.; Scuseria, G. E.; Halas, N. J.; Wong, M. S., Observing Metal-Catalyzed Chemical Reactions in Situ Using Surface-Enhanced Raman Spectroscopy on Pd−Au Nanoshells. *J. Am. Chem. Soc.* **2008**, *130*, 16592-16600.

[13] Zou, S.; Williams, C. T.; Chen, E. K. Y.; Weaver, M. J., Surface-Enhanced Raman Scattering as a Ubiquitous Vibrational Probe of Transition-Metal Interfaces: Benzene and Related Chemisorbates on Palladium and Rhodium in Aqueous Solution. *J. Phys. Chem. B* **1998**, *102*, 9039-9049.

[14] Grass, M. E.; Zhang, Y.; Butcher, D. R.; Park, J. Y.; Li, Y.; Bluhm, H.; Bratlie, K. M.; Zhang, T.; Somorjai, G. A., A Reactive Oxide Overlayer on Rhodium Nanoparticles during CO Oxidation and Its Size Dependence Studied by In Situ Ambient-Pressure X-ray Photoelectron Spectroscopy. *Angew. Chem. Int. Ed.* **2008**, *47*, 8893-8896.

[15] Dolamic, I.; Bürgi, T., Photoassisted Decomposition of Malonic Acid on TiO2 Studied by in Situ Attenuated Total Reflection Infrared Spectroscopy. *J. Phys. Chem. B* **2006**, *110*, 14898-14904.

[16] Mojet, B. L.; Ebbesen, S. D.; Lefferts, L., Light at the interface: the potential of attenuated total reflection infrared spectroscopy for understanding heterogeneous catalysis in water. *Chem. Soc. Rev.* **2010**, *39*, 4643-4655.

[17] Chen, T.; Feng, Z.; Wu, G.; Shi, J.; Ma, G.; Ying, P.; Li, C., Mechanistic Studies of Photocatalytic Reaction of Methanol for Hydrogen Production on Pt/TiO2 by in situ Fourier Transform IR and Time-Resolved IR Spectroscopy. *J. Phys. Chem. C* **2007**, *111*, 8005-8014.

[18] Brownson, J. R. S.; Tejedor-Tejedor, M. I.; Anderson, M. A., FTIR Spectroscopy of Alcohol and Formate Interactions with Mesoporous TiO2 Surfaces. *J. Phys. Chem. B* **2006**, *110*, 12494-12499.

[19] Cremer, P. S.; Su, X.; Shen, Y. R.; Somorjai, G. A., Hydrogenation and Dehydrogenation of Propylene on Pt(111) Studied by Sum Frequency Generation from UHV to Atmospheric Pressure. *J. Phys. Chem.* **1996**, *100*, 16302-16309.

[20] Tinnemans, S. J.; Mesu, J. G.; Kervinen, K.; Visser, T.; Nijhuis, T. A.; Beale, A. M.; Keller, D. E.; van der Eerden, A. M. J.; Weckhuysen, B. M., Combining operando techniques in one spectroscopic-reaction cell: New opportunities for elucidating the active site and related reaction mechanism in catalysis. *Catal. Today* **2006**, *113*, 3-15.

[21] Wang, Y.; Wöll, C., Chemical reactions on metal oxide surfaces investigated by vibrational spectroscopy. *Surface Science* **2009**, *603*, 1589-1599.

[22] Fan, F.; Feng, Z.; Li, C., UV Raman Spectroscopic Studies on Active Sites and Synthesis Mechanisms of Transition Metal-Containing Microporous and Mesoporous Materials. *Acc. Chem. Res.* **2009**, *43*, 378-387.

[23] Weckhuysen, B. M., Snapshots of a working catalyst: possibilities and limitations of in situ spectroscopy in the field of heterogeneous catalysis. *Chem. Commun.* **2002**, 97-110.

[24] Banares, M. A., Operando methodology: combination of in situ spectroscopy and simultaneous activity measurements under catalytic reaction conditions. *Catal. Today* **2005**, *100*, 71-77.

[25] Foster, A. J.; Lobo, R. F., Identifying reaction intermediates and catalytic active sites through in situ characterization techniques. *Chem. Soc. Rev.* **2010**, *39*, 4783-4793.

[26] Kneipp, K.; Wang, Y.; Kneipp, H.; Perelman, L. T.; Itzkan, I.; Dasari, R. R.; Feld, M. S., Single Molecule Detection Using Surface-Enhanced Raman Scattering (SERS). *Phys. Rev. Lett.* **1997**, *78*, 1667.

[27] Nie, S.; Emory, S. R., Probing Single Molecules and Single Nanoparticles by Surface-Enhanced Raman Scattering. *Science* **1997**, *275*, 1102-1106.

[28] Xu, H.; Bjerneld, E. J.; Käll, M.; Börjesson, L., Spectroscopy of Single Hemoglobin Molecules by Surface Enhanced Raman Scattering. *Phys. Rev. Lett.* **1999**, *83*, 4357.

[29] Rycenga, M.; McLellan, J. M.; Xia, Y., Controlling the assembly of silver nanocubes through selective functionalization of their faces. *Adv. Mater.* **2008**, *20*, 2416-2419.

[30] Stewart, M. E.; Anderton, C. R.; Thompson, L. B.; Maria, J.; Gray, S. K.; Rogers, J. A.; Nuzzo, R. G., Nanostructured plasmonic sensors. *Chem. Rev.* **2008**, *108*, 494-521.

[31] Banholzer, M. J.; Millstone, J. E.; Qin, L.; Mirkin, C. A., Rationally designed nanostructures for surface-enhanced Raman spectroscopy. *Chem. Soc. Rev.* **2008**, *37*, 885-897.

[32] Tao, A.; Sinsermsuksakul, P.; Yang, P., Tunable plasmonic lattices of silver nanocrystals. *Nature Nanotech.* **2007**, *2*, 435-440.

[33] Camden, J. P.; Dieringer, J. A.; Wang, Y.; Masiello, D. J.; Marks, L. D.; Schatz, G. C.; Van Duyne, R. P., Probing the Structure of Single-Molecule Surface-Enhanced Raman Scattering Hot Spots. *J. Am. Chem. Soc.* **2008**, *130*, 12616-12617.

[34] Camden, J. P.; Dieringer, J. A.; Zhao, J.; Van Duyne, R. P., Controlled Plasmonic Nanostructures for Surface-Enhanced Spectroscopy and Sensing. *Acc. Chem. Res.* **2008**, *41*, 1653-1661.

[35] Yan, B.; Thubagere, A.; Premasiri, W. R.; Ziegler, L. D.; Dal Negro, L.; Reinhard, B. M., Engineered SERS Substrates With Multiscale Signal Enhancement: Nanoplarticle Cluster Arrays. *ACS Nano* **2009**, *3*, 1190-1202.

[36] Lassiter, J. B.; Aizpurua, J.; Hernandez, L. I.; Brandl, D. W.; Romero, I.; Lal, S.; Hafner, J. H.; Nordlander, P.; Halas, N. J., Close encounters between two nanoshells. *Nano Lett.* **2008**, *8*, 1212-1218.

[37] Henzie, J.; Andrews, S. C.; Ling, X. Y.; Li, Z.; Yang, P., Oriented assembly of polyhedral plasmonic nanoparticle clusters. *Proc Natl Acad Sci U S A* **2013**, *110*, 6640-6645.

[38] Mulvihill, M.; Tao, A.; Benjauthrit, K.; Arnold, J.; Yang, P., Surface-Enhanced Raman Spectroscopy for Trace Arsenic Detection in Contaminated Water. *Angew. Chem. Int. Ed.* **2008**, *47*, 6456-6460.

[39] McLellan, J. M.; Siekkinen, A.; Chen, J.; Xia, Y., Comparison of the surface-enhanced Raman scattering on sharp and truncated silver nanocubes. *Chem. Phys. Lett.* **2006**, *427*, 122-126.

[40] Mulvihill, M. J.; Ling, X. Y.; Henzie, J.; Yang, P. D., Anisotropic Etching of Silver Nanoparticles for Plasmonic Structures Capable of Single-Particle SERS. *J. Am. Chem. Soc.* **2010**, *132*, 268-274.

[41] Camargo, P. H. C.; Rycenga, M.; Au, L.; Xia, Y., Isolating and Probing the Hot Spot Formed between Two Silver Nanocubes. *Angew. Chem. Int. Ed.* **2009**, *48*, 2180-2184.

[42] Hardcastle, F. D.; Ishihara, H.; Sharma, R.; Biris, A. S., Photoelectroactivity and Raman spectroscopy of anodized titania (TiO2) photoactive water-splitting catalysts as a function of oxygen-annealing temperature. *J. Mater. Chem.* **2011**, *21*, 6337-6345.

[43] Yang, C.-C.; Yu, Y.-H.; van der Linden, B.; Wu, J. C. S.; Mul, G., Artificial Photosynthesis over Crystalline TiO2-Based Catalysts: Fact or Fiction? *J. Am. Chem. Soc.* **2010**, *132*, 8398-8406.

[44] Selloni, A., Crystal growth: Anatase shows its reactive side. *Nature Mater.* **2008**, *7*, 613-615.

[45] D'Arienzo, M.; Carbajo, J.; Bahamonde, A.; Crippa, M.; Polizzi, S.; Scotti, R.; Wahba, L.; Morazzoni, F., Photogenerated Defects in Shape-Controlled TiO2 Anatase Nanocrystals: A Probe To Evaluate the Role of Crystal Facets in Photocatalytic Processes. J. *Am. Chem. Soc.* **2011**, *133*, 17652-17661.

[46] Yang, H. G.; Sun, C. H.; Qiao, S. Z.; Zou, J.; Liu, G.; Smith, S. C.; Cheng, H. M.; Lu, G. Q., Anatase TiO2 single crystals with a large percentage of reactive facets. *Nature* **2008**, *453*, 638-641.

[47] Serpone, N.; Martin, J.; Horikoshi, S.; Hidaka, H., Photocatalyzed oxidation and mineralization of C1–C5 linear aliphatic acids in UV-irradiated aqueous titania dispersions—kinetics, identification of intermediates and quantum yields. *J. Photochem. Photobiol. A* **2005**, *169*, 235-251.

[48] Ohsaka, T.; Izumi, F.; Fujiki, Y., Raman spectrum of anatase, TiO2. *J. Raman Spectrosc.* **1978**, *7*, 321-324.

[49] Nakamoto, K., *Infrared and Raman Spectra of Inorganic and Coordination Compounds: Theory and applications in inorganic chemistry,* Wiley-VCH: Weinheim, 2009.

[50] Lin, W. Y.; Frei, H., Photochemical and FT-IR probing of the active site of hydrogen peroxide in Ti silicalite sieve. *J. Am. Chem. Soc.* **2002**, *124*, 9292-9298.

[51] Zhang, J.; Li, M.; Feng, Z.; Chen, J.; Li, C., UV Raman Spectroscopic Study on TiO2. I. Phase Transformation at the Surface and in the Bulk. *J. Phys. Chem. B* **2005**, *110*, 927-935.

[52] Nakamura, R.; Imanishi, A.; Murakoshi, K.; Nakato, Y., In situ FTIR studies of primary intermediates of photocatalytic reactions on nanocrystalline TiO2 films in contact with aqueous solutions. *J. Am. Chem. Soc.* **2003**, *125*, 7443-7450.

[53] Connor, P. A.; Dobson, K. D.; McQuillan, A. J., Infrared spectroscopy of the TiO2/aqueous solution interface. *Langmuir* **1999**, *15*, 2402-2408.

[54] Tao, A.; Sinsermsuksakul, P.; Yang, P. D., Polyhedral silver nanocrystals with distinct scattering signatures. *Angew. Chem. Int. Ed.* **2006**, *45*, 4597-4601.

[55] Zhang, Y.; Grass, M. E.; Habas, S. E.; Tao, F.; Zhang, T.; Yang, P.; Somorjai, G. A., One-step Polyol Synthesis and Langmuir−Blodgett Monolayer Formation of Size-tunable Monodisperse Rhodium Nanocrystals with Catalytically Active (111) Surface Structures. *J. Phys. Chem. C* **2007**, *111*, 12243-12253.

[56] Tao, A. R.; Huang, J.; Yang, P., Langmuir−Blodgettry of Nanocrystals and Nanowires. *Acc. Chem. Res.* **2008**, *41*, 1662-1673.

[57] Song, H.; Kim, F.; Connor, S.; Somorjai, G. A.; Yang, P., Pt Nanocrystals: Shape Control and Langmuir−Blodgett Monolayer Formation. *J. Phys. Chem. B* **2004**, *109*, 188-193.

Electronic Supplementary Material

Alumina Coated Ag Nanocrystal Monolayer as Surface-Enhanced Raman Spectroscopy Platforms for Direct Spectroscopic Detection of Water Splitting Reaction Intermediates

Xing Yi Ling[1,#, †], Ruoxue Yan[1,#, ††], Sylvia Lo[1], Dat Tien Hoang[1], Chong Liu[1], Melissa A. Fardy[1], Sher Bahadar

Khan[2], Abdullah M. Asiri[2], Salem M. Bawaked[2], Peidong Yang[1,2] (✉)

[1] Department of Chemistry, University of California, Berkeley, CA, United States

[2] Center of Excellence for Advanced Materials Research (CEAMR), King Abdulaziz University, Jeddah 21589, P.O. Box 80203, Saudi Arabia

† Present address: Division of Chemistry and Biological Chemistry, School of Physical and Mathematical Sciences, Nanyang Technological University, Singapore

†† Present address: Department of Chemical and Environmental Engineering. University of California, Riverside, CA, United States # These authors contributed equally to this work

INFORMATION ABOUT ELECTRONIC SUPPLEMENTARY MATERIAL. The font is Palatino Linotype 10. Electronic supplementary material (ESM) may include large artwork, lengthy descriptions, and extensive data. Each supporting information artwork, description, and data file should be referred to in the manuscript at least once. The format is "Fig. S-1 in the Electronic Supplementary Material (ESM)", or "Figure S-2 in the ESM" at the beginning of a sentence. A brief description of the ESM should be included in the main text, before the references section, in a paragraph entitled "Electronic Supplementary Material:". ESM should be submitted with the manuscript and will be sent to referees during peer review. Authors should ensure that it is clearly presented.

_____

Address correspondence to p_yang@berkeley.edu

Figure S-1. Dark field scattering spectrum of a cubic Ag nanoparticle.

Figure S-2. (a) Raman spectra of as prepared Ag cube, O_2 plasma cleaned Ag cube, and O_2 plasma cleaned Ag cube upon rinsing in aminothiophenol solution. (b) Raman spectra of aminothiophenol on Ag LB film with and without O_2 plasma treatment, showing that the cleaning procedure do not degrade the SERS performance of the Ag film. (c) Raman spectra of alumina-coated O_2 plasma-cleaned Ag nanocubes (Ag SERS platform), and TiO_2 deposited Ag SERS platform.

Figure S-3. Steady State SERS spectra during water splitting reaction under pH 10 condition after 120 mins of UV irradiation.
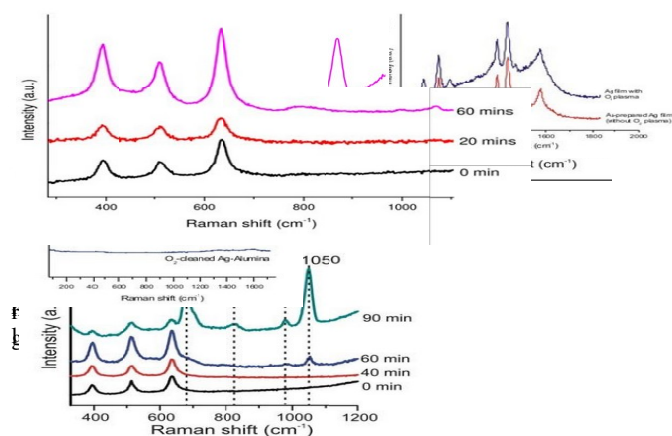

Figure S-4. SERS spectra collected on a different sample, showing the onset of the intermediate peaks at 60 mins. Water splitting reaction was carried out under pH 10 and data was collected up to 60 mins of UV irradiation.
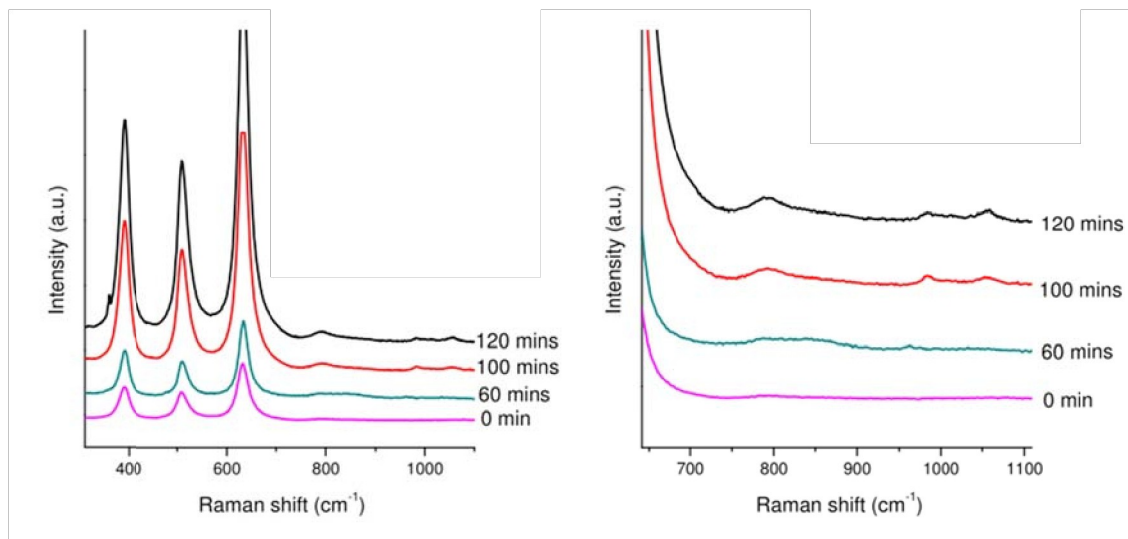
Figure S-5. SERS spectra collected on Commercial Anatase Powders during water splitting reaction under pH 10 under UV irradiation of up to 120 mins. The commercial anatase powders have much larger sizes, which mean that a large portion of the surface sites is inaccessible to SERS enhancement and weak intermediate signals are expected. Nonetheless, it has shown similar spectral features as the anatase TiO_2 nanoplate, although the 680 cm^{-1} peak was overwhelmed by the strong photon mode from the large anatase particles.